Eur. Phys. J. D **22**, 501–512 (2003)
DOI: 10.1140/epjd/e2003-00045-5

THE EUROPEAN PHYSICAL JOURNAL D

Multimode squeezed states produced by a confocal parametric oscillator

K.I. Petsas[1], A. Gatti[1,a], L.A. Lugiato[1], and C. Fabre[2]

[1] INFM, Università dell'Insubria, Dipartimento di Scienze CC FF MM, Via Valleggio 11, 22100 Como, Italy
[2] Laboratoire Kastler Brossel, Université Pierre et Marie Curie, Case 74, 75252 Paris Cedex 05, France

Received 25 September 2002
Published online 11 February 2003 –

Abstract. We investigate the spatial behaviour of the quantum-noise-reduction spectrum of the vacuum state emitted by a degenerate optical parametric oscillator below threshold. In view of possible experimental implementations, we consider a mode–degenerate resonator and two matching lenses and show that, for the realistic case of a finite–width pump, significant level of squeezing can be observed in a very small region of the beam.

PACS. 42.50.Dv Nonclassical field states; squeezed, antibunched, and sub-Poissonian states; operational definitions of the phase of the field; phase measurements – 42.65.Yj Optical parametric oscillators and amplifiers – 42.60.Da Resonators, cavities, amplifiers, arrays, and rings

1 Introduction

In the last few years there has been an increasing interest towards the spatial aspects of nonclassical light. This interest mainly arises from the possibility of using spatial quantum properties of light beam in order to improve the quality of image processing, or, more in general, for parallel processing of information at the quantum level (see [1] for a recent review on this subject). Recent proposals include the use of locally squeezed light beams, that is, beams which display quantum noise reduction in several portions of the transverse section, in order to increase the resolution of image detection [2]; the possibility of improving the sensitivity of the measurement of small beam displacements by exploiting spatial nonclassical correlations in the beam cross-section [3,4]; the possibility of quantum teleportation of an optical image, or in general, parallel teleportation of quantum information by using either local squeezing or local entanglement [5].

Most of the literature on squeezed states of radiation concerns squeezing which occurs in a spatially singlemode beam, and treats only temporal aspects of the issue [6]. Some pioneering work regarding the investigation of spatial effects in squeezing appeared in the last decade [7–11]. It has been shown, in particular, for the case of an optical parametric oscillator (OPO) that the observed level of squeezing exhibits a crucial dependence on the quality of matching between the transverse configurations of the deamplified signal beam and of the local oscillator field (LO) [9]. A first attempt to provide a description of the spatial structure of squeezed states has been exposed in [10,11], where again a close connection between the degree of squeezing and the spatial configuration of the LO has been pointed out.

It is clear that in a spatially singlemode beam, in order to detect a good level of squeezing, not only the LO must be matched to the spatial mode but also the whole beam must be detected. If the size of the detection region is gradually decreased with respect to the transverse beam size, the level of squeezing is gradually degraded because more and more spatial modes, which are not squeezed, come into play. In order to have squeezing in small portions of the transverse cross-section, it is necessary to generate a *spatially multimode* squeezed state, that is, to have a significant level of squeezing over a broad band of spatial modes.

Kolobov and Sokolov [7] were the first to address the issue of "local" squeezing. They showed that efficient quantum noise reduction can be observed even in small regions of the output signal beam of a single-pass parametric amplifier, provided that the size of the detection region is not smaller than the inverse of the spatial bandwidth of the amplifier. This hence introduces a lower limit for the dimension of the area over which squeezing can be observed (coherence area). However, the generation of spatially multimode squeezed light from travelling wave amplifiers presents a main problem: homodyne detection is difficult to perform, because of the difficulty of matching the LO spectral profile to the huge bandwidth of the amplifier.

An ideal candidate for generating multimode squeezed light is rather parametric down-conversion taking place

[a] e-mail: alessandra.gatti@mi.infn.it

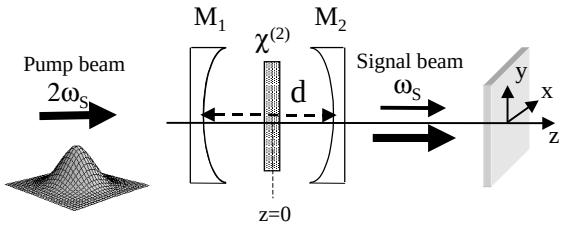

Fig. 1. Scheme of a confocal Fabry-Perot OPO. The two spherical mirrors are separated by a distance d equal to their radius of curvature R. At the signal frequency ω_s, mirror M_2 has a high reflectivity, while M_1 has 100% reflectivity. Both mirrors transmit the pump field at frequency $2\omega_s$.

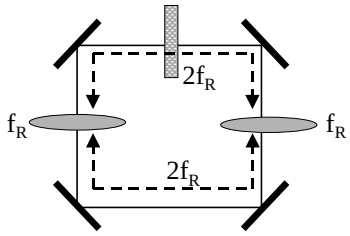

Fig. 2. Equivalent ring cavity configuration. The two lenses have a focal length $f_R = R/2$.

in a mode-degenerate cavity. A first investigation in this sense was performed in reference [13], where the case of a confocal optical parametric oscillator below threshold was analyzed and where it was shown that, under appropriate conditions, the observed level of squeezing may become independent of the spatial profile of the LO. As a consequence, one finds the same level of squeezing in any *arbitrarily small* region of the output beam, provided it is symmetrical with respect to the cavity axis.

In this paper, in view of possible experimental implementations, we formulate a more realistic description of the generation of squeezed light by a confocal OPO. In particular we release the unrealistic assumption of a plane-wave driving pump of the model studied in [13]. Finite-size pump effects in OPOs have been considered only in recent theoretical studies [15–17], where it was shown that the finiteness of the pump may dramatically alter the degree of observability of some major spatial features of the OPO. In the case of the confocal OPO, not surprisingly, we find that if the pump waist is decreased starting from the plane wave configuration, the level of squeezing is degraded and also depends on the shape of the LO used to probe the squeezing. However, the interesting feature is that, by reducing the size of the detection region, the level of squeezing *improves*, and, for a small enough region, the level of squeezing of the plane-wave theory is recovered together with the independence from the LO shape.

Moreover, we investigate the impact of the finite size of some optical elements, and the effects of small deviations from the ideal confocal geometry. The main effects is in both cases to introduce a finite resolution in the system, so that efficient squeezing is recovered when detecting light from small but not arbitrarily small regions.

The paper is organized as follows. In Section 2 we review in more detail a quantum model for parametric down-conversion in a confocal cavity that was already presented in [14], for the purpose of studying the noiseless amplification of images in such a device. Section 3 describes the detection scheme and introduces the spectrum of squeezing in the case of the confocal cavity geometry. In Section 4 we perform numerical investigations for the level of squeezing in the case of a Gaussian pump profile and for several values of the pump width, in the ideal case of a perfect confocal geometry and infinite resolution. The effect of finite resolution of the system is examined by introducing a finite-size pupil in Section 5. Section 6 is devoted to investigate the case of an imperfect confocal geometry. We show, also in this realistic situation, that for small deviation from confocality the salient features presented in Section 4 are still preserved.

2 Quantum model for the confocal OPO below threshold

We consider parametric down-conversion taking place inside a confocal cavity, formed by two spherical mirrors separated by a distance d equal to their radius of curvature R, as in the scheme of Figure 1. Figure 2 shows the equivalent ring cavity configuration, where the two mirrors are replaced by two lenses of focal length $f_R = d/2$, symmetrically placed along the cavity length, and separated by a distance $2f_R$. The cavity contains in its center a thin optical parametric $\chi^{(2)}$ medium. The overall setup is coherently driven by a pump field A_P of frequency $2\omega_s$. We assume type I, collinear, and degenerate phase matching conditions inside the crystal, so that the pump field is partially downconverted by the parametric interaction to a signal field of half frequency ω_s.

For what concerns the signal field, we assume that only one of the cavity mirror is partially transparent, while the other is totally reflecting at the frequency ω_s. For the pump, we assume that the cavity mirrors are totally transparent at frequency $2\omega_s$, so that the injected pump field only travels along the cavity once. At difference from the analysis of [13] the pump is allowed to have an arbitrary spatial transverse profile, that in most of the paper will be taken as Gaussian, corresponding to a beam waist w_P at the cavity center:

$$\overline{A}_P(\mathbf{x}, z=0) = \overline{A}_P \exp\left(-r^2/w_P^2\right). \tag{1}$$

In the framework of paraxial and slowly varying approximation, the signal field envelope is slowly varying with respect to a carrier $\exp(\mathrm{i}k_s z - \mathrm{i}\omega_s t)$, k_s being the signal wave-number at frequency ω_s. Because of the cylindrical symmetry along Oz, the resonator supports a set of Gauss-Laguerre modes [18], as eigenmodes for the the signal field envelope. By denoting the cylindrical coordinates as $r = \sqrt{x^2 + y^2}$ and ϕ, and by taking the reference plane $z = 0$ at the cavity center, in the region *e.g.* between the

cavity center and the right mirror they have the form:

$$f_{pl}(r,\phi,z) = R_{pl}(r,z)\frac{\mathrm{e}^{(\mathrm{i}l\phi)}}{\sqrt{2\pi}}\exp\left[\mathrm{i}\left(\frac{z}{z_r}\frac{r^2}{w(z)^2} - \theta_{pl}(z)\right)\right], \tag{2}$$

where $p = 0, 1, 2...$ is the radial index and $l = 0, \pm 1, ...$ is the angular index. The radial part of the modes is given by:

$$R_{pl}(r,z) = \frac{2}{w(z)}\left(2\frac{r^2}{w(z)^2}\right)^{\frac{|l|}{2}} \times L_p^{|l|}\left(2\frac{r^2}{w(z)^2}\right)\exp\left[-\frac{r^2}{w(z)^2}\right], \tag{3}$$

z_r being the Rayleigh range of the resonator ($z_r = d/2$ for the confocal resonator), and $w(z) = w_0\left(1 + z^2/z_r^2\right)^{1/2}$ being the signal beam waist at distance z from the cavity center. The functions $L_p^{|l|}$ are Laguerre polynomials of the indicated indices [19]. The phase factor θ_{pl} arises because of propagation along Oz, and has the form:

$$\theta_{pl}(z) = (2p + |l| + 1)\tan^{-1}\left(\frac{z}{z_r}\right). \tag{4}$$

The special feature of a confocal resonator is that complete sets of Gauss-Laguerre modes with a given parity (even or odd) with respect to transverse coordinate inversion gather into frequency degenerate families [18], characterized by the integer index $n = 2m + 2p + l$, where m (the longitudinal index) is an integer that plays no special role in the following. The frequency separation between the families is equal to one half the free spectral range.

One of the main assumption of our model is that only one of these families, for definiteness one corresponding to l even, is close to the frequency of the signal field, while all the others are far away and do not contribute to the dynamics. Let us denote with ω_c the frequency of the resonant mode family having the index $n = n_c$. This family contains an infinite number of even Gauss-Laguerre modes, that satisfy a completeness relation of the form

$$\sum_{p,l}^{l\ \text{even}} f_{p,l}^*(\mathbf{x},z) f_{p,l}(\mathbf{x}',z) = \delta_+(\mathbf{x},\mathbf{x}'), \tag{5}$$

where we introduced the symmetrized Dirac delta functions

$$\delta_\pm(\mathbf{x},\mathbf{x}') = \frac{1}{2}\left[\delta(\mathbf{x}-\mathbf{x}') \pm \delta(\mathbf{x}+\mathbf{x}')\right]. \tag{6}$$

This set of modes form a complete and orthonormal basis for any function of the transverse coordinates even with respect to coordinate inversion in the transverse plane.

Let us introduce the envelope operator of the intracavity field over the modes of the resonant family, in the following way

$$B_+(\mathbf{x},t) = {\sum_{p,l}}' f_{p,l}(\mathbf{x},z=0)a_{p,l}(t), \quad \text{for } z = 0, \tag{7}$$

where ${\sum}'_{p,l}$ denotes a sum over the modes of the resonant family, with an even parity, and $a_{p,l}(t)$ indicate mode operators, obeying the usual equal time commutation relations:

$$\left[a_{p,l}(t), a_{p',l'}^\dagger(t)\right] = \delta_{p,p'}\delta_{l,l'}. \tag{8}$$

Our model is derived in the framework of the mean field limit [20], that basically assumes that the parametric interaction is very weak in a single pass through the nonlinear medium, but the cavity lifetime is long enough (the outcoupling mirror transmittivity is small) that the cumulative effect of many passages in the crystal is not negligible. Moreover, we assume here that the crystal is thin, *i.e.* much shorter than the resonator Rayleigh range. This allows us to consider the fields constant along the crystal length. Moreover, being interested in the system dynamics below the threshold for parametric oscillation, the pump depletion along the crystal is in this condition negligible and we shall describe the pump field as a c-number classical field.

Under these assumption the Hamiltonian describing the parametric interaction can be written in the form [11]

$$H_{\mathrm{int}} = \frac{\mathrm{i}\hbar g}{2}\int \mathrm{d}\mathbf{x}\left\{\overline{A}_P(\mathbf{x})\left[B_+^\dagger(\mathbf{x},t)\right]^2 - \overline{A}_P^*(\mathbf{x})\left[B_+(\mathbf{x},t)\right]^2\right\}, \tag{9}$$

where g is the coupling constant, proportional to the second order nonlinear susceptibility $\chi^{(2)}$ and to the crystal length. In writing this Hamiltonian we assumed that the pump has a transverse profile even with respect to the coordinate inversion $\overline{A}_P(-\mathbf{x}) = \overline{A}_P(\mathbf{x})$, and we neglected the contribution of all the other cavity modes that belong to families far away from resonance. The form of the interaction Hamiltonian has been closely examined in reference [17] for the particular case of a pump with Gaussian profile in the plane transverse to the propagation direction and for a spherical, quasi-planar mirror geometry of the resonator. Because of the finite spatial extent of the pump, intermode couplings occur in the cavity due to the parametric interaction. By introducing the intracavity field expansion (7) in (9) we get:

$$H_{\mathrm{int}} = \frac{\mathrm{i}\hbar}{2}{\sum_{pl}}'{\sum_{p',l'}}'\left[g_{p,l:p'l'}a_{pl}^\dagger a_{p'l'}^\dagger - g_{p,l;p'l'}^* a_{pl}a_{p'l'}\right], \tag{10}$$

with the intermode coupling coefficients given by

$$g_{p,l;p'l'} = g\int \mathrm{d}\mathbf{x}\ f_{p,l}^*(\mathbf{x},z=0)f_{p',l'}^*(\mathbf{x},z=0)\overline{A}_P(\mathbf{x}). \tag{11}$$

As a result, the system cannot be simply characterized by a set of independent one-mode optical parametric oscillators, in contrast to the case of a plane wave pump.

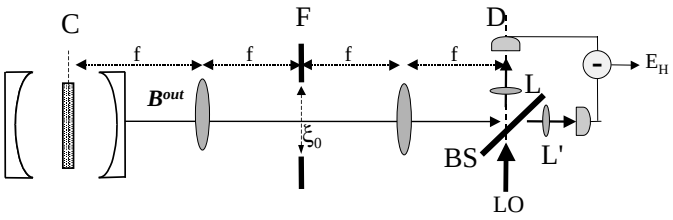

Fig. 3. Balanced homodyne detection scheme. Two matching lenses of focal length f are used to image the cavity centre C at the detection plane D. Planes C, F (far field-plane) and D are minimum waist planes for the signal beam. The detection plane is imaged on the two photodetectors by identical lenses L and L'. We assume that the detection plane D is a minimum waist plane for the Gaussian LO (the LO phase is constant in this plane).

The free evolution of the intracavity signal field is described as usual by a Hamiltonian term of the form:

$$H_{\text{free}} = \sum_{p,l}{}' \hbar \left(\omega_{pl} - \omega_s\right) a_{pl}^{\dagger} a_{pl} \tag{12}$$

$$= \hbar\gamma\Delta \int \mathrm{d}\mathbf{x}\; B_+^{\dagger}\left(\mathbf{x},t\right) B_+\left(\mathbf{x},t\right), \tag{13}$$

where in passing from the first to the second line we used the fact that, thanks to the confocal geometry, all the modes of the resonant family are degenerate in frequency, $\omega_{pl} = \omega_c$, and we introduced the cavity detuning $\Delta = (\omega_c - \omega_s)/\gamma$, scaled to the cavity linewidth γ.

In the framework of standard cavity input/output formalism [22], the intracavity field dynamics is described by a Langevin equation for the time-evolution of the signal operator at the crystal/cavity center

$$\frac{\partial}{\partial t} B_+\left(\mathbf{x},t\right) = -\gamma\left[\left(1+\mathrm{i}\Delta\right) B_+\left(\mathbf{x},t\right) - A_P\left(\mathbf{x}\right) B_+^{\dagger}\left(\mathbf{x},t\right)\right] + \sqrt{2\gamma} B_+^{\text{in}}\left(\mathbf{x},t\right) \tag{14}$$

where we expressed the pump field as a dimensionless space-dependent parameter $A_P(\mathbf{x}) = (g/\gamma)\overline{A}_P(\mathbf{x})$, in such a way that the pump amplitude is normalized to its threshold value for parametric oscillation in the plane wave limit ($A_P = 1$ at threshold for $w_P \to \infty$).

Here $B_+^{\text{in}}(\mathbf{x},t)$ denotes the part of the input field operator even with respect to the inversion of the transverse coordinate. More precisely we introduce even and odd input/output operators as

$$B_{\pm}^{\text{in/out}}(\mathbf{x},t) = \frac{1}{2}\left[B^{\text{in/out}}(\mathbf{x},t) \pm B^{\text{in/out}}(-\mathbf{x},t)\right], \tag{15}$$

where for example $\mathbf{x}$ is in the upper semiplane. $B_{\pm}^{\text{in/out}}$ represent the envelope operators of the input/output fields calculated at the cavity center $z = 0$ (more precisely, they represent the input/output operators calculated at the detection plane of Figure 3, where the cavity center is imaged). They obey the following commutation relations

$$\left[B_{\pm}^{\text{in/out}}(\mathbf{x},t), B_{\pm}^{\text{in/out}\dagger}(\mathbf{x}',t')\right] = \frac{1}{2}\Big[\delta\left(\mathbf{x}-\mathbf{x}'\right) \pm \delta\left(\mathbf{x}+\mathbf{x}'\right)\Big]\delta(t-t'), \tag{16}$$

$$\left[B_{\pm}^{\text{in/out}}(\mathbf{x},t), B_{\mp}^{\text{in/out}\dagger}(\mathbf{x}',t)\right] = 0. \tag{17}$$

In addition we have to consider the relation linking the outgoing fields $B_{\pm}^{\text{out}}(\mathbf{x},t)$ with the intracavity and input fields at the cavity input/output port [22]

$$B_{\pm}^{\text{out}}(\mathbf{x},t) = \sqrt{2\gamma} B_{\pm}(\mathbf{x},t) - B_{\pm}^{\text{in}}(\mathbf{x},t). \tag{18}$$

Equation (14) is easily solved in the frequency domain. Taking into account the boundary condition (18) we obtain

$$B_+^{\text{out}}(\mathbf{x},\Omega) = \mathcal{U}(\mathbf{x},\Omega) B_+^{\text{in}}(\mathbf{x},\Omega) + \mathcal{V}(\mathbf{x},\Omega) B_+^{\text{in}\,\dagger}(\mathbf{x},-\Omega), \tag{19}$$

where

$$B_{\pm}^{\text{in/out}}(\mathbf{x},\Omega) = \int \frac{\mathrm{d}t}{\sqrt{2\pi}} B_{\pm}^{\text{in/out}}(\mathbf{x},t)\mathrm{e}^{-\mathrm{i}\Omega t}, \tag{20}$$

and

$$\mathcal{U}(\mathbf{x},\Omega) = \frac{\left[1-\mathrm{i}\left(\Delta-\Omega/\gamma\right)\right]\left[1-\mathrm{i}\left(\Delta+\Omega/\gamma\right)\right] + A_p^2(\mathbf{x})}{\left[1+\mathrm{i}\left(\Delta+\Omega/\gamma\right)\right]\left[1-\mathrm{i}\left(\Delta-\Omega/\gamma\right)\right] - A_p^2(\mathbf{x})}, \tag{21}$$

$$\mathcal{V}(\mathbf{x},\Omega) = \frac{2A_p(\mathbf{x})}{\left[1+\mathrm{i}\left(\Delta+\Omega/\gamma\right)\right]\left[1-\mathrm{i}\left(\Delta-\Omega/\gamma\right)\right] - A_p^2(\mathbf{x})}. \tag{22}$$

Notice that a simple phase shift relates the output odd part of the field to the input one, since we assumed that only intracavity modes with even parity are resonant and subject to a significant nonlinear mixing.

The input-output relation (19) describes an infinite set of independent optical parametric oscillators below threshold, one for each couple of symmetric points in the transverse plane $\mathbf{x}$ and $-\mathbf{x}$. The distance from threshold of each OPO, and hence the amount of squeezing, is related to the pump amplitude in the same point. The fact that each pair of symmetric transverse positions is uncoupled from the others is a direct consequence of the confocal geometry, that eliminates the effects of field diffraction during intracavity propagation.

3 Homodyne detection and squeezing spectrum

The method which is mainly used for measuring the noise-spectrum outside the cavity is a balanced homodyne detection scheme [6]. The complete detection scheme

is schematically shown in Figure 3. The two matching lenses of focal length f have the role of imaging the crystal/cavity center plane C onto the detection plane D. The image focal plane F of the first lens coincides with the object focal plane of the second one, and represents the far-field plane with respect to the cavity center C. In planes C, F, D the signal field has its minimum waist, and it has a flat wavefront. The lenses are able to compensate for the different propagation-induced phase-shifts θ_{pl} of the Gauss Laguerre modes at the detection plane. A detailed expression of these phase-shifts can be found in the Appendix A.

At the plane D the symmetrical beam-splitter BS (reflection and transmission coefficients $r = 1/\sqrt{2}$ and $t = 1/\sqrt{2}$) mixes the output signal field with an intense, stationary and coherent beam $\alpha_L(\mathbf{x}, z)$, usually called local oscillator (LO). Note that all the fields being evaluated at the beam-splitter location, we will omit the z-dependence in the following. The beams emerging from the beam-splitter are then imaged by identical lenses L and L' on the photodetectors surface, and the resulting photocurrents subtracted. The difference photocurrent is a measure of the quadrature operator (homodyne field):

$$E_H(\Omega) = \int_{s_{\rm det}} \mathrm{d}\mathbf{x}\,[B^{\rm out}(\mathbf{x},\Omega)\alpha_L^*(\mathbf{x}) + B^{\rm out\dagger}(\mathbf{x},-\Omega)\alpha_L(\mathbf{x})], \quad (23)$$

where $s_{\rm det}$ is the reciprocal image of the photodetection region at the beamsplitter plane, and assumed to be identical for the two photodetectors. We have also assumed here that the quantum efficiency of the photodetector is equal to 1. Here

$$B^{\rm out}(\mathbf{x},\Omega) = B_+^{\rm out}(\mathbf{x},\Omega) + B_-^{\rm out}(\mathbf{x},\Omega) \quad (24)$$

is the total output signal field, sum of its even and odd parts.

The fluctuations $\delta E_H(\Omega)$ of the homodyne field around steady state are characterized by a noise-spectrum:

$$V(\Omega) = \int_{-\infty}^{+\infty} \mathrm{d}\Omega'\ \langle \delta E_H(\Omega)\,\delta E_H(\Omega')\rangle \quad (25)$$

$$= N + S(\Omega), \quad (26)$$

where N is the mean photon number measured by the detector

$$N = \int_{s_{\rm det}} \mathrm{d}\mathbf{x}\ |\alpha_L(\mathbf{x})|^2, \quad (27)$$

N represents the shot-noise level, that is the noise level of a coherent state, and we have denoted by S the normally ordered part of the fluctuation spectrum, which accounts for the excess or decrease of noise with respect to coherent states.

4 Squeezing spectrum in the ideal case: infinite resolution

Let us first consider the ideal confocal case, in which the resolution of the system is not limited by any finite size optical element.

Since we assumed that the odd part of the output field is in the vacuum state, $B_-^{\rm out}$ gives no contribution to the normally ordered part of the spectrum S, which can be calculated by using the input/output relation (19) for the even part of the field, and the commutation rules for the even input (16). By assuming a local oscillator that has an even parity with respect to coordinate inversion $\alpha_L(\mathbf{x}) = \alpha_L(-\mathbf{x})$, we get:

$$S(\Omega) = \int_{s_{\rm det}} \mathrm{d}\mathbf{x} \int_{s_{\rm det}} \mathrm{d}\mathbf{x}'\delta_+(\mathbf{x},\mathbf{x}')\,|\alpha_L(\mathbf{x})|^2 \times \left\{|\mathcal{V}(\mathbf{x},\Omega)|^2 + |\mathcal{V}(\mathbf{x},-\Omega)|^2 + 2\mathcal{R}e\left[\mathrm{e}^{-2\mathrm{i}\varphi_L(\mathbf{x})}\mathcal{U}(\mathbf{x},\Omega)\,\mathcal{V}(\mathbf{x},-\Omega)\right]\right\}, \quad (28)$$

where $\varphi_L(\mathbf{x})$ is the phase distribution of the LO at plane D.

By noticing that that due to the unitarity of the input/output transformation (19), functions $\mathcal{U}$ and $\mathcal{V}$ satisfy

$$|\mathcal{U}(\mathbf{x},\Omega)|^2 - |\mathcal{V}(\mathbf{x},\Omega)|^2 = 1, \quad (29)$$

$$\mathcal{U}(\mathbf{x},\Omega)\mathcal{V}(\mathbf{x},-\Omega) = \mathcal{U}(\mathbf{x},-\Omega)\mathcal{V}(\mathbf{x},\Omega) \rightarrow |\mathcal{V}(\mathbf{x},\Omega)|^2 = |\mathcal{V}(\mathbf{x},-\Omega)|^2 \quad (30)$$

(as can be easily verified from their explicit expression), we can finally recast the noise spectrum in the more compact form:

$$V(\Omega) = \int_{s_{\rm det}} \mathrm{d}\mathbf{x}\left\{|\alpha_L(\mathbf{x})|^2\,[1-\sigma(\mathbf{x})]\right\} + \int_{s_{\rm det}} \mathrm{d}\mathbf{x}\left\{|\alpha_L(\mathbf{x})|^2\,\sigma(\mathbf{x})R(\mathbf{x},\Omega)\right\}, \quad (31)$$

$$R(\mathbf{x},\Omega) = \left|\mathcal{U}(\mathbf{x},\Omega) + \mathrm{e}^{2\mathrm{i}\varphi_L(\mathbf{x})}\mathcal{V}^*(\mathbf{x},-\Omega)\right|^2. \quad (32)$$

In this equation we have introduced the geometrical factor

$$\sigma(\mathbf{x}) = \int_{s_{\rm det}} \mathrm{d}\mathbf{x}'\delta_+(\mathbf{x},\mathbf{x}') \quad (33)$$

that accounts for the shape of the detection region. The function $R(\mathbf{x},\Omega)$ is the noise spatial density, and it approaches zero in point $\mathbf{x}$ for a proper choice of the local oscillator phase in that point and for a large enough gain. In fact, if the LO phase is chosen as $\varphi_L(\mathbf{x}) = 1/2\arg[-\mathcal{U}(\mathbf{x},\Omega)\mathcal{V}(\mathbf{x},-\Omega)]$

$$R(\mathbf{x},\Omega) = [|\mathcal{U}(\mathbf{x},\Omega)| - |\mathcal{V}(\mathbf{x},\Omega)|]^2 = \frac{1}{[|\mathcal{U}(\mathbf{x},\Omega)| + |\mathcal{V}(\mathbf{x},\Omega)|]^2}. \quad (34)$$

At resonance, for $\Delta = 0$, and at zero frequency, the noise density has an especially simple expression

$$R(\mathbf{x},\Omega=0) = \left[\frac{1-A_p(\mathbf{x})}{1+A_p(\mathbf{x})}\right]^2. \quad (35)$$

for $\varphi_L(\mathbf{x}) = \pi/2$.

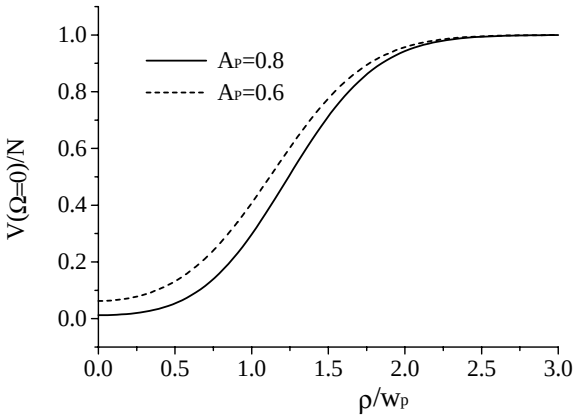

Fig. 4. Detection from two small symmetric pixels. Squeezing spectrum at zero-frequency, normalized to the shot-noise, as a function of the pixel distance ρ from the cavity axis, scaled to the pump beam waist. Plane wave LO, $\Delta = 0$; solid line $A_P = 0.8$; dashed line $A_P = 0.6$.

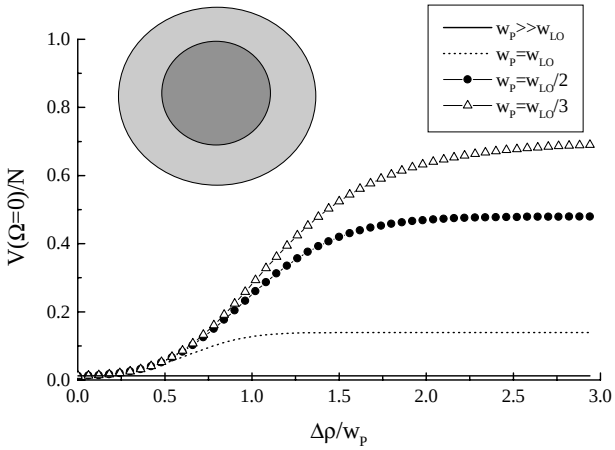

Fig. 5. Squeezing spectrum at zero-frequency, normalized to the shot-noise, as a function of the radial amplitude of the detector (scaled to the waist of the pump w_P) for $A_P = 0.8$ and for $\Delta = 0$. The figure corresponds to Gaussian pump and LO and has been plotted for several values of the ratio $w_P/w_{\rm LO}$.

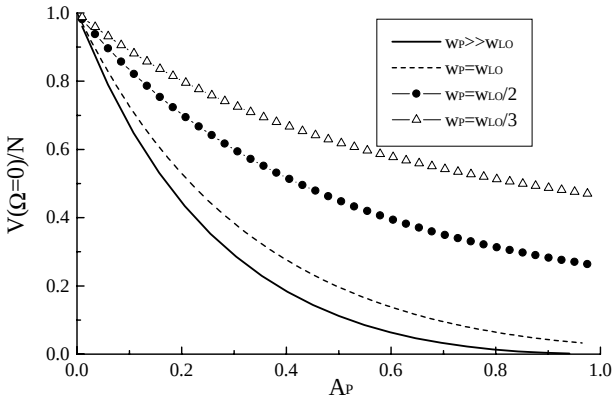

Fig. 6. Squeezing spectrum at zero-frequency (normalized to the shot-noise) as a function of A_P for $\Delta = 0$. The figure corresponds to a Gaussian pump and LO and has been plotted for several values of the ratio $w_P/w_{\rm LO}$. The radial amplitude of the detector is $\Delta\rho = 3w_{\rm LO}$.

We notice that only when the detection region is symmetric, $\sigma(\mathbf{x}) = 1$ for any $\mathbf{x}$ inside the detection region, and there is the possibility of beating the shot noise. However, for a completely non-symmetric region, like a single pixel placed not on the symmetry axis, $\sigma(\mathbf{x}) = 1/2$, and the noise spectrum cannot be reduced below $N/2$. The reason is that in the case of a nonsymmetric detection region, the vacuum fluctuations of the odd part of the field come into play, while they cancel out when summing the contributions coming from two symmetrical regions of the transverse plane.

In the following we shall assume, as in [13] that the LO at plane D, where it is mixed with the signal beam, has a constant phase profile $\varphi_L(\mathbf{x}) = \varphi_L$. In the limit of a plane-wave pump, the noise density becomes constant over the transverse plane $R(\mathbf{x}, \Omega) \to R^{\rm PW}(\Omega)$, and it can be taken out from the integral in equation (31). By considering a symmetric detection region, the level of squeezing, when scaled to the shot noise level, becomes completely independent of the shape and size of both the local oscillator and the detection region.

$$V(\Omega)^{\rm PW} = NR^{PW}(\Omega). \tag{36}$$

In this way the results of [13], which were derived in the framework of a different but equivalent model, are recovered. Note that, implicit in this result, is the fact that the transverse plane can be divided in arbitrary small regions, and the light detected from any two symmetric regions shows the same level of squeezing as the light detected from the whole beam.

In the more realistic case of a finite-size pump, the detected level of squeezing depends on the shape and position of the detection region. The case of two small symmetric pixels (pixel size much smaller than the pump waist) is illustrated in Figure 4, which has been obtained for a PW LO. As it should be clear from equation (35) the level of obtainable squeezing is large only in the region of the transverse plane where there is significant gain, and reaches the shot-noise level where the pump vanishes. We outline that this apparently obvious result is only a consequence of the fact that diffraction has been eliminated by the confocal geometry.

Figures 5 and 6 show instead results for a measurement performed with a circular detector of radial amplitude $\Delta\rho$ centered on the cavity axis, and a Gaussian LO characterized by by a beam waist $w_{\rm LO}$

$$\alpha_L(\mathbf{x}) = |\alpha_L| e^{i\varphi_L} \exp\left(-|\mathbf{x}|^2/w_{\rm LO}^2\right). \tag{37}$$

at the plane D.

Figure 5 represents the squeezing spectrum at zero-frequency, for a fixed value of the input pump ($A_P = 0.8$) as a function of the radius $\Delta\rho$ of the detection region, normalized to the waist of the pump. As pointed out in reference [13], for a plane-wave driving pump the observed

level of squeezing does not depend on the width of the detection region. This is illustrated by the solid line curve of Figure 5, which corresponds to $w_P \gg w_{\rm LO}$. For a narrower pump (dashed, circles and triangle curves) the level of squeezing now depends both on the LO and and the detection region size. Remarkably, the level of squeezing improves for a smaller detection region, and it becomes close to the ideal plane-wave level when the detection region is small compared to the pump spot size. Moreover, when $\Delta\rho$ is small enough, all the lines tend to the same value, and the observed squeezing should become independent of the LO shape.

Figure 6 represents the squeezing spectrum $V(\Omega = 0)/N$, as a function of the input pump amplitude, for several values of the pump to LO waist ratios $w_P/w_{\rm LO}$. These curves correspond to a relatively broad detection region, characterized by $\Delta\rho = 3w_{\rm LO}$. The solid line curve of the figure corresponds to the plane-wave pump ($w_P \gg w_{\rm LO}$). When considering a finite-size pump (dashed and dot curves) the observed level of squeezing lies above the ideal plane-wave-limit. However, it may be seen that even for realistic values of the pump waist (*i.e.* for w_P on the order of $w_{\rm LO}$) the squeezing spectrum is relatively close to the plane-wave-pump limit.

5 Squeezing spectrum in the finite resolution case

Until now we have considered an optical system that has infinite resolution, and we have shown that in such a case the observed level of squeezing can be optimized in an arbitrarily small detection region. This is equivalent to say that our system is able to support an infinite number of transverse modes, of arbitrary large order. In a realistic system, optical elements have a finite transverse size, and this implies that higher order modes are cut off, so that resolution is finite. As it has been shown in reference [7], because of the finite resolution, there is a lower limit for $\Delta\rho$ under which there is not efficient squeezing. A simple way to account for the finite resolution of the system is to introduce a finite-size circular aperture of radius ξ_0 in plane F, midway between the two imaging lenses (see Fig. 3).

Straightforward calculations, reported in Appendix B, show then that the input/output relation is no more point by point as in equation (19), but rather is in the form of a convolution integral that links all the points in a spatial region of size on the order of the diffraction spot $s_{\rm diff} \sim (\lambda f)^2/(\pi\xi_0^2)$ of the aperture on the detector. Only when the detection region $s_{\rm det}$ is quite large compared to the diffraction spot of the aperture, the same result is recovered as in the case of infinite optical resolution given by equation (31), indepedentely of the radius of the aperture.

On the other hand, in the limit where the detection region $s_{\rm det}$ is much narrower than the diffraction spot $s_{\rm diff}$ one finds:

$$V(\Omega) \simeq N + \frac{s_{\rm det}}{s_{\rm diff}} S^{\rm PW}(\Omega), \tag{38}$$

where $S^{\rm PW}(\Omega)$ is the plane-wave result obtained in the case of infinite resolution. In the limit of infinitely small detection region equation (38) shows that the observed level of squeezing tends to the shot-noise. We can hence conclude that when taking into account the finite resolution of the system, the detection region cannot be arbitrarily small in order to observe efficient quantum noise reduction.

6 Beyond the ideal case: imperfect confocality

In this section we examine an even more realistic situation, where the confocality of the cavity is not perfect. This situation is of particular interest in view of experimental applications, where the limit of ideal confocality cannot be achieved with an arbitrary accuracy. We evaluate numerically how a small deviation from confocality influences the observed level of squeezing, especially for narrow detection regions. We show that in this situation, even in the absence of any finite size optical element, the system has finite resolution.

In the case where the cavity is not perfectly confocal, the Langevin equations for the temporal evolution of the signal field can no longer be put in the simple form of equations (14), the major effect of a small deviation from confocality being to introduce diffraction in the system. We consider a small deviation from the confocal geometry by letting the radius of curvature of the mirrors be slightly different from their distance

$$R = d + \delta R, \qquad |\delta R| \ll d \tag{39}$$

with δR positive or negative. The effect is to remove the ideal mode degeneracy, so that the modes of the quasi-resonant family have a frequency $\omega_{pl} = \omega_{00} + (2p+l)\Delta\,\Omega$, where the mode separation is given by

$$\begin{aligned} \frac{\delta\Omega}{\gamma} &= \frac{FSR}{2\gamma}\left[\frac{4}{\pi}\tan^{-1}\sqrt{\frac{d}{2R-d}} - 1\right] \\ &\approx -\frac{FSR}{\pi\gamma}\frac{\delta R}{d} \approx \frac{1}{T}\frac{\delta R}{d}, \end{aligned} \tag{40}$$

with FSR being the cavity free spectral range, and T the transmission coefficient of the outcoupling mirror. From this formula we see that when $\delta R/d \ll T$, the frequency separation of the modes of the quasi-resonant family is much smaller than the cavity linewidth. Still a large number of transverse mode frequencies are inside the cavity bandwidth, and we are allowed to limit our description to the even modes of the quasi-resonant family, and to neglect those of other mode families that are frequency separated by more than a half free spectral range.

The free Hamiltonian (13) has to be modified as:

$$H_{\text{free}} = \sum_{p,l}{}' \hbar\left(\omega_{pl} - \omega_s\right) a_{pl}^{\dagger} a_{pl} \tag{41}$$

$$= \hbar \int \mathrm{d}\mathbf{x} B_+^{\dagger}(\mathbf{x}, z) \left[\omega_{00} - \omega_s - \delta\Omega\left(\frac{w_c^2}{4}\nabla_{\perp}^2 - \frac{|\mathbf{x}|^2}{w_c^2}\right)\right] B_+(\mathbf{x}, z) \tag{42}$$

where the second line was obtained with the help of the standard eigenvalue equation for Gauss Laguerre modes [19].

The intracavity field dynamics is now governed by the following Langevin equation

$$\frac{\partial}{\partial t} B_+(\mathbf{x}, t) = -\gamma\left[1 + \mathrm{i}\Delta - \mathrm{i}\frac{\delta\Omega}{\gamma}\left(\frac{w_c^2}{4}\nabla_{\perp}^2 - \frac{|\mathbf{x}|^2}{w_c^2}\right)\right] B_+(\mathbf{x}, t) + \gamma A_P(\mathbf{x}) B_+^{\dagger}(\mathbf{x}, t) + \sqrt{2\gamma} B_+^{\text{in}}(\mathbf{x}, t). \tag{43}$$

As in similar equations, derived for a quasi-planar or planar cavities [12], the transverse Laplacian $\nabla_{\perp}^2$ models the effect of diffraction during intracavity propagation, and introduces coupling among different points in the transverse plain. Clearly, as one gets close to the confocal point $\delta\Omega \to 0$, and different transverse points (besides the two symmetrical ones) become dynamically decoupled.

However, we didn't solve the dynamical equation in the form of (43) but rather considered the intracavity field expansion on Gauss-Laguerre modes (7) and derived the equation for the time evolution of mode operators

$$\frac{\mathrm{d}}{\mathrm{d}t} a_{pl}(t) = -\gamma\left(1 + \mathrm{i}\Delta_{pl}\right) a_{pl}(t) + \gamma A_P \sum_{p'l'} g_{pl;p'l'} a_{p'l'}^{\dagger}(t) + \sqrt{2\gamma} a_{pl}^{\text{in}}(t). \tag{44}$$

Here $g_{pl;p'l'}$ are the intermode coupling coefficients given by equation (11), a_{pl}^{in} are vacuum input mode operators, and we introduced the resonator mode detunings $\Delta_{pl} = (\omega_{pl} - \omega_s)/\gamma = \Delta + (2p + l)\delta\Omega/\gamma$.

Notice that since we assumed a Gaussian pump (in general this is true for any pump with cylindrical symmetry) $g_{pl;p'l'} = \delta_{l,-l'} g_{pl;p'-l}$ and the dynamical equation (44) couples only modes with opposite helicity, or, in a more sophisticated language, modes which carry opposite angular momentum.

The numerical method for solving equations (44) has been presented in detail in [17]. We consider a finite-set of transverse modes and express the Langevin equations (44) in Fourier frequency-space. Making use of the standard input–output formalism [22] the operators for the output signal field are linked to the ones of the input field in a closed-set of coupled algebraic linear equations. From these equations the matrix of second order moments of the output mode operators can be numerically calculated from that of the input mode operators, which are in the vacuum state.

When considering squeezing, it is more convenient to consider an alternative Gauss-Laguerre mode basis defined, for $l > 0$, as:

$$h_{pl1}(r, \phi, z) = \frac{f_{pl}(r, \phi, z) + f_{p-l}(r, \phi, z)}{\sqrt{2}} \propto \cos(\phi) \tag{45}$$

$$h_{pl2}(r, \phi, z) = \frac{f_{pl}(r, \phi, z) - f_{p-l}(r, \phi, z)}{\mathrm{i}\sqrt{2}} \propto \sin(\phi). \tag{46}$$

By introducing the numerical coefficients:

$$\rho_{pli} \mathrm{e}^{\mathrm{i}\varphi_{pli}} = \int_{s_{\text{det}}} \mathrm{d}\mathbf{x}\ \alpha_L(\mathbf{x}) h_{pli}^*(\mathbf{x}, z_D), \tag{47}$$

where z_D is the coordinate of plane D (see Fig. 3), one is able to recast the squeezing spectrum (25) in the following form:

$$V(\Omega) = N + \sum_{p,l,i}{}' \sum_{p'} \rho_{pli}\rho_{p'li} S_{pli;p'li}(\Omega), \tag{48}$$

where $\sum_{p,l,i}'$ stands for the sum over cavity modes with l even and where we introduced the two-mode squeezing spectrum [17]:

$$S_{pli;p'li}(\Omega) = 2\Re e\left\{\mathrm{e}^{\mathrm{i}(\varphi_{pli} - \varphi_{p'li})} \int_{-\infty}^{\infty} \mathrm{d}\Omega'\ \left\langle a_{pli}^{\dagger\text{out}}(-\Omega) a_{p'li}^{\text{out}}(\Omega')\right\rangle + \mathrm{e}^{-\mathrm{i}(\varphi_{pli} + \varphi_{p'li})} \int_{-\infty}^{\infty} \mathrm{d}\Omega'\ \left\langle a_{pli}^{\text{out}}(\Omega) a_{p'li}^{\text{out}}(\Omega')\right\rangle\right\}. \tag{49}$$

A detailed expression of the phase factors φ_{pli} can be found in Appendix A. We incidentally note the following normalization property:

$$\sum_{p,l,i} \rho_{pli}^2 = \int_{s_{\text{det}}} \mathrm{d}\mathbf{x}\ |\alpha_L(\mathbf{x})|^2 = N. \tag{50}$$

From the point of view of the numerical implementation, we considered maximum cutoff mode-indices $p_{\max}$ and $l_{\max}$ (with $l_{\max}$ even). This is justified by the fact that the finite-size of the optical intracavity elements, as well as the diffraction losses in the resonator limit the total number of involved Gauss Laguerre modes.

Figure 7 illustrates the variation of the squeezing spectrum at zero-frequency, for a fixed value of the input pump ($A_P = 0.8$) as a function of the radius $\Delta\rho$ of the detection region in the case of a small deviation from confocality. In Figure 7a the transverse mode spacing is $\delta\Omega = 0.05\gamma$, whereas in Figure 7b $\delta\Omega = 0.01\gamma$. The general behaviour of the squeezing spectrum is similar to that of Figure 5; however, it can be seen immediately on both figures that in the limit of a very small detector size, the observed level of noise increases rapidly, similarly to the finite resolution case examined in the previous section. Reason for this is that when detecting light from a small region of the transverse plane, the fluctuations of high order modes, that vary on a small spatial scale, come into play. Since modes are no

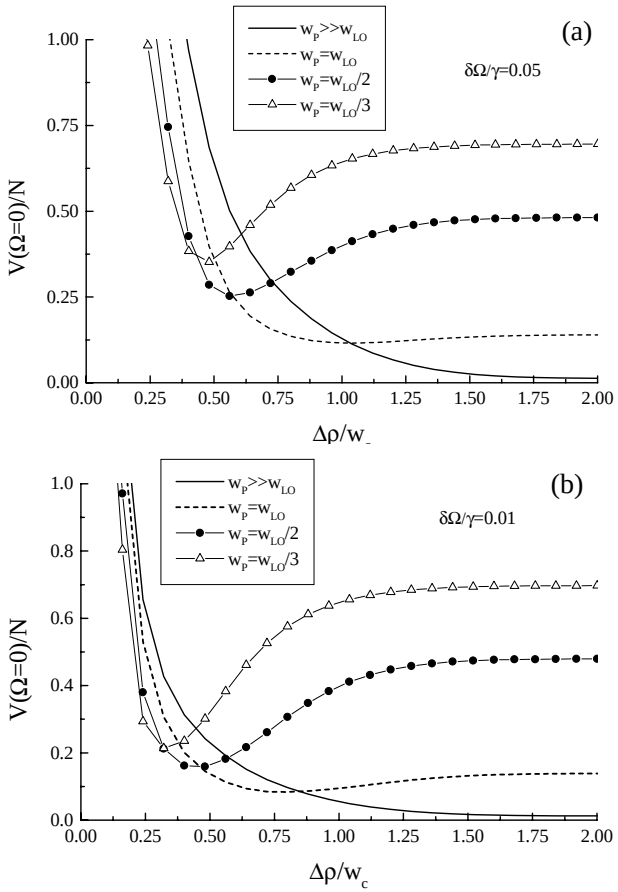

Fig. 7. Small deviations from the confocal geometry. Squeezing spectrum at zero-frequency, normalized to the shot-noise, as a function of the radial amplitude of the detector for $A_P = 0.8$ and for $\Delta = 0$. (a) $\delta\Omega = 0.05\gamma$, (b) $\delta\Omega = 0.01\gamma$. The radius of the detector is scaled to the cavity waist w_c. The figure corresponds to Gaussian pump and LO, with $w_{\rm LO}{=}w_c$ and has been plotted for several values of the ratio $w_P/w_{\rm LO}$).

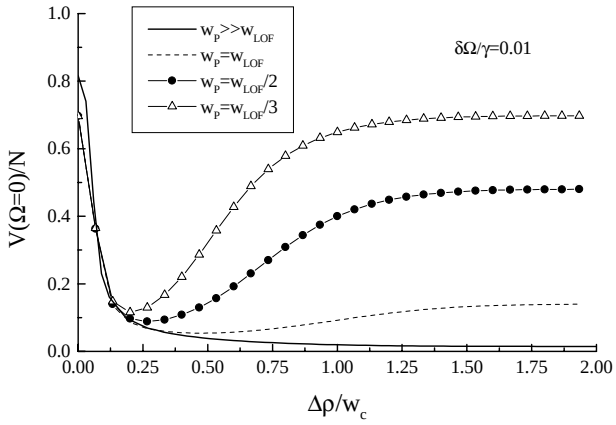

Fig. 8. Same as Figure 7b, with the squeezing spectrum optimized by shifting the detection plane by an amount $\delta z = -[\delta\Omega/(\gamma(1+A_p^2))]z_r$, and assuming a LO mode-matched to the TEM_{00} cavity mode at that plane. Notice the improvement of the squeezing level with respect to Figure 7b, when detecting light from small detection regions.

more at degeneracy, higher order modes are more far away from resonance than low order modes (we assumed here that the fundamental TEM_{00} mode is at resonance) and hence the level of squeezing of their fluctuations is lower. Even more important, the squeezing ellipses of the various modes are no more aligned along the same axis, as in the degenerate case, but they are slightly rotated with respect to that of the TEM_{00} mode. This means that, if the LO phase is chosen as to detect the most squeezed quadrature for TEM_{00} mode, for higher order modes the quadrature detected will be no more the most squeezed one, but eventually the most amplified one, which results in a excess of noise with respect to shot noise. This is clearly shown by the fact the the curves of Figure 7 go above the shot noise level when the detection region becomes very small. These effects are more relevant for a larger pump, since a narrow pump limits the available gain to low order modes, whose spatial distribution is concentrated close to the cavity axis.

However, there is a trick to partially compensate for the rotation of the various squeezing ellipses, which consists of shifting the detection plane D by an amount $\delta z (|\delta z| \ll z_R)$. When δz is properly chosen, as we will show below, the results shown in Figure 8 are obtained. When it is compared with the analogue Figure 7b, which was obtained in the absence of any optimization of the detection plane position, it shows a significant improvement of the level of squeezing obtained by detecting light in a narrow spatial region. In particular, all the curves lye now below the shot noise, even for extremely narrow detection region. The drawback is however, that in order to optimize the scheme, the LO oscillator must be exactly mode-matched to the TEM_{00} cavity mode at the detection plane.

The squeezing ellipse rotation can be estimated in the case of a plane-wave pump, where the two-mode squeezing spectra (49) reduce to single-mode spectra and can be analytically calculated. We obtain

$$\lim_{w_p/w_c\to\infty} S_{pli;p'li}\left(\Omega\right) = \delta_{p,p'} S_{pli}\left(\Omega\right) \tag{51}$$

$$S_{pli}\left(\Omega\right) = 2\Re e\left\{\left|\mathcal{V}_{pl}\left(\Omega\right)\right|^2 + \mathrm{e}^{-2\mathrm{i}\varphi_{pli}}\mathcal{U}_{pl}\left(\Omega\right)\mathcal{V}_{pl}\left(-\Omega\right)\right\} \tag{52}$$

with $\mathcal{U}_{pl}\left(\Omega\right)$, $\mathcal{V}_{pl}\left(\Omega\right)$ given by the expressions (21, 22), respectively, with the substitution $\Delta_+ \to \Delta_{pl}$ and $A_P(\mathbf{x}) \to A_P$. These spectra are minimized, at zero frequency, by the choice

$$2\varphi_{pli}^{\min} = \arg\left[-\mathcal{U}_{pl}(0)\mathcal{V}_{pl}(0)\right] \approx \pi - \frac{2\Delta_{pl}}{1+A_p^2} = \pi - 2(2p+|l|)\frac{\delta\Omega}{\gamma(1+A_p^2)}, \tag{53}$$

for small detuning parameters Δ_{pl}. The propagation phase shifts of the various modes are calculated in Appendix B, and as a result (Eq. (60)) $2\varphi_{pli} = 2\varphi_{\rm LO} + 2\left(2p+|l|\right)\tan^{-1} z/z_R$.

Considering small z/z_R, optimal compensation of the squeezing ellipse rotation is in the plane wave case achieved for

$$\frac{\delta z}{z_R} \approx -\frac{\delta\Omega}{\gamma(1+A_p^2)}\cdot \tag{54}$$

7 Conclusions

In this paper we have investigated a confocal OPO below threshold, as an ideal device for producing multimode squeezed light, for which the a good level of squeezing is present in small portions of the beam cross-section. We have considered several realistic situations (finite extent of the pump, finite optical resolution, imperfect confocality) which are of interest in view of experimental implementations.

Mode-degenerate cavities offer the possibility of an especially simple treatment, because they are *diffractionless*. In the framework of an ideal mode-degenerate geometry, we have shown that the finite size of the driving pump alters the ideal picture of [13], in the sense that the level of detected squeezing for a narrow pump depends both on the LO shape and on the size of the detection region. However, by detecting light from small detection region well inside the pump transverse profile, we have shown that the ideal plane wave results can be recovered.

Small deviations from the confocal geometry and the presence of finite size optical elements introduce a finite resolution in the system, by limiting the number of spatial modes which have a significant squeezing. This in turns imposes a lower limit on the size of the detection region where efficient squeezing is present. However, for realistic deviations from the ideal geometry, the minimum size of this region is still much smaller than the cavity waist.

One of the limitations of our analysis is the fact that the detection region must be symmetric in order to detect good squeezing; if a non-symmetric detection region is used, as a single pixel not on the cavity axis, the noise cannot be reduced below half of the shot noise level. This is a consequence of the confocal geometry, for which the cavity resonances correspond to degenerate families of modes with even or odd parity. Clearly the best situation would be that of a resonator for which a complete set of spatial modes is at degeneracy, *i.e.* of a self-imaging resonator, which can be realized in ring cavities analogous to Figure 2, and using for example three plane mirrors and three lenses separated by their focal length, or four plane mirrors and three lenses separated by three times their focal length.

This subject, together with the important issue of the effects of using a thick crystal, inside which diffraction cannot be neglected, will be the subject of a forthcoming publication.

This work was supported by the network QSTRUCT and the project QUANTIM (IST 2000 26019) of respectively the TMR and the FET programmes of the European Union.

Appendix A: Matching scheme and propagation induced phase-shifts for the squeezing spectrum

In this appendix we examine more closely the two-lens matching scheme of Figure 3 and we analyze the propagation induced phase-shift of the signal field in terms of phase-shifts on the Gauss Laguerre resonator modes.

A Gaussian beam, of Rayleigh range z_r and waist $w_c = \sqrt{\lambda z_r/\pi}$, which has its minimum waist at plane C, is transformed by the first lens into a Gaussian beam with its minimum waist at plane F. Rayleigh ranges and waists in planes C and F are related by $z_r z_r^F = f^2$ and $w_F w_c = (\lambda f/\pi)^2$. Propagation phase shifts undergone by mode f_{pl} during its propagation from plane C to plane F through the lens are:

$$\begin{aligned}\theta_{pl}(\mathrm{C}\to\mathrm{F}) &= (2p+|l|+1)\left[\tan^{-1}\frac{f}{z_r}+\tan^{-1}\frac{z_r}{f}\right]\\ &= (2p+|l|+1)\frac{\pi}{2}\cdot\end{aligned} \tag{55}$$

In a similar way, the second lens transforms a Gaussian beam having its minimum waist in plane C into a Gaussian beam having its minimum waist in plane D, where the beam Rayleigh range is $z_r^D = f^2/z_r^C = z_R$. The propagation phase shifts are:

$$\begin{aligned}\theta_{pl}(\mathrm{F}\to\mathrm{D}) &= (2p+|l|+1)\left[\tan^{-1}\frac{z_r}{f}+\tan^{-1}\frac{f}{z_R}\right]\\ &= (2p+|l|+1)\frac{\pi}{2}\cdot\end{aligned} \tag{56}$$

Hence the total phase shifts from plane C to plane D are $\theta_{pl}(\mathrm{C}\to\mathrm{D}) = (2p+|l|+1)\pi$, in agreement with the fact that the two lens telescopic system transforms whatever field distribution $\alpha_C(\mathbf{x})$ in plane C to the symmetric field distribution $\alpha_D(\mathbf{x}) = -\alpha_C(-\mathbf{x})$.

As a result, assuming a flat LO wavefront in plane D, the phase factors appearing in equations (47, 49) are:

$$\varphi_{pli} = \varphi_{\mathrm{LO}} + (2p+|l|+1)\,\pi, \tag{57}$$

$$\varphi_{p_1 li} - \varphi_{p_2 li} = 2\,(p_1-p_2)\,\pi = 0 \pmod{2\pi} \tag{58}$$

$$\begin{aligned}\varphi_{p_1 li} + \varphi_{p_2 li} &= 2\varphi_{\mathrm{LO}} + 2\,(p_1+p_2+|l|+1)\,\pi\\ &= 2\varphi_{\mathrm{LO}} \pmod{2\pi}.\end{aligned} \tag{59}$$

Let us now consider the case where the local oscillator is mixed with the signal field at a plane D′ shifted from D by an amount z, with z positive or negative. By assuming that the LO is mode-matched with the TEM_{00} cavity mode, the phase profile $\propto (z/z_r)(r^2/w\,(z)^2)$ accounting for the wavefront curvature of the modes (see Eq. (2)) is compensated by the LO wavefront curvature, and the phase factors of equations (47), appearing in equation (52) are

$$\begin{aligned}2\varphi_{pli} &= 2\varphi_{\mathrm{LO}} + [\theta_{pl}(\mathrm{C}\to\mathrm{D}') - \theta_{00}(\mathrm{C}\to\mathrm{D}')]\\ &= 2\varphi_{\mathrm{LO}} + 2\,(2p+|l|)\tan^{-1}\frac{z}{z_R}\cdot\end{aligned} \tag{60}$$

Appendix B

To describe correctly the effect of the pupil, one has to consider the propagation of the light field through the optical setup in two steps: the first lens provides a spatial Fourier transform of the output field $B_{\rm out}(\mathbf{x},\Omega)$, so that at the location of the pupil the field is

$$\widetilde{B}_{\rm out}\left(\boldsymbol{\xi},\Omega\right)=\frac{1}{\lambda f}\int \mathrm{d}\mathbf{x}' B_{\rm out}\left(\mathbf{x}',\Omega\right)\exp\left(-\mathrm{i}\frac{2\pi}{\lambda f}\mathbf{x}'\cdot\boldsymbol{\xi}\right); \tag{61}$$

similarly, the effect of the second lens is to provide a spatial Fourier transform of the field $\widetilde{B}_{\rm out}(\boldsymbol{\xi},\Omega)$ at the focal image plane so that the field at the location of the LO is:

$$\mathcal{E}\left(\mathbf{x},\Omega\right)=\frac{1}{\lambda f}\int \mathrm{d}\boldsymbol{\xi} P\left(\boldsymbol{\xi}\right)\widetilde{B}_{\rm out}\left(\boldsymbol{\xi},\Omega\right)\exp\left(-\mathrm{i}\frac{2\pi}{\lambda f}\mathbf{x}'\cdot\boldsymbol{\xi}\right), \tag{62}$$

where $P\left(\boldsymbol{\xi}\right)$ is the pupil function given by:

$$P\left(\boldsymbol{\xi}\right)=1 \text{ if } |\boldsymbol{\xi}|\leq\xi_0,\ P\left(\boldsymbol{\xi}\right)=0 \text{ else.} \tag{63}$$

By expressing $\widetilde{B}_{\rm out}(\boldsymbol{\xi},\Omega)$ in terms of its inverse Fourier transform one obtains:

$$\mathcal{E}\left(\mathbf{x},\Omega\right)=\frac{1}{\lambda f}\int \mathrm{d}\mathbf{x}' g\left(\mathbf{x}+\mathbf{x}'\right)B_{\rm out}\left(\mathbf{x}',\Omega\right), \tag{64}$$

where we have introduced the pupil frame function

$$g\left(\mathbf{x}\right)=\frac{1}{\lambda f}\int \mathrm{d}\boldsymbol{\xi} P\left(\boldsymbol{\xi}\right)\exp\left(-\mathrm{i}\frac{2\pi}{\lambda f}\mathbf{x}'\cdot\boldsymbol{\xi}\right). \tag{65}$$

In the limit of infinitely large pupil, one recovers the infinite resolution case, since $g\left(\mathbf{x}\right)=\lambda f\delta(\mathbf{x})$ and $\mathcal{E}(\mathbf{x},\Omega)=B_{\rm out}(\mathbf{x},\Omega)$. Again, using the input-output relations (19) in equation (64) it is possible to express the signal field at the location of the LO $\mathcal{E}$ as a function of the input field $B_{\rm in}$. Using the fact that the pupil frame function varies on a spatial scale which is on the order of $\lambda f/\xi_0$, whereas the functions $\mathcal{U}$ and $\mathcal{V}$ of equation (19) vary on a larger spatial scale, it is possible to write:

$$\begin{aligned}\mathcal{E}\left(\mathbf{x},\Omega\right)\simeq&\frac{1}{\lambda f}\mathcal{U}\left(\mathbf{x},\Omega\right)\int \mathrm{d}\mathbf{x}' g\left(\mathbf{x}+\mathbf{x}'\right)B_{\rm in}\left(\mathbf{x}',\Omega\right)\\&+\frac{1}{\lambda f}\mathcal{V}\left(\mathbf{x},\Omega\right)\int \mathrm{d}\mathbf{x}' g\left(\mathbf{x}+\mathbf{x}'\right)B_{\rm in}^{\dagger}\left(\mathbf{x}',-\Omega\right).\end{aligned} \tag{66}$$

The homodyne field is given by equation (23), but replacing $\mathcal{E}$ for $B_{\rm out}$:

$$E_H^{\rm out}\left(\Omega\right)=\int_{s_{\rm det}}\mathrm{d}\mathbf{x}\ \left[\mathcal{E}\left(\mathbf{x},\Omega\right)\alpha_L^*\left(\mathbf{x}\right)+\mathcal{E}^{\dagger}\left(\mathbf{x},-\Omega\right)\alpha_L\left(\mathbf{x}\right)\right]. \tag{67}$$

Using the parity of the functions $\mathcal{U}$ and $\mathcal{V}$ and the following properties of the pupil frame function:

$$\int \mathrm{d}\mathbf{x}_1\ g\left(\mathbf{x}+\mathbf{x}_1\right)g\left(\mathbf{x}'+\mathbf{x}_1\right)=\lambda f g\left(\mathbf{x}-\mathbf{x}'\right),$$

$$\int \mathrm{d}\mathbf{x}_1\ g\left(\mathbf{x}+\mathbf{x}_1\right)g\left(\mathbf{x}'-\mathbf{x}_1\right)=\lambda f g\left(\mathbf{x}+\mathbf{x}'\right),$$

we can cast the general expression of the squeezing spectrum in the presence of the aperture:

$$\begin{aligned}V\left(\Omega\right)=N+\int_{s_{\rm det}}\mathrm{d}\mathbf{x}\int_{s_{\rm det}}\mathrm{d}\mathbf{x}'\mathcal{R}e\Big\{&\alpha_L\left(\mathbf{x}\right)\alpha_L^*\left(\mathbf{x}'\right)\mathcal{V}^*\left(\mathbf{x},-\Omega\right)\\&\times\mathcal{V}\left(\mathbf{x}',-\Omega\right)\left[\frac{g\left(\mathbf{x}-\mathbf{x}'\right)}{\lambda f}+\frac{g\left(\mathbf{x}+\mathbf{x}'\right)}{\lambda f}\right]+\alpha_L^*\left(\mathbf{x}\right)\alpha_L^*\left(\mathbf{x}'\right)\\&\times\mathcal{U}\left(\mathbf{x},\Omega\right)\mathcal{V}\left(\mathbf{x}',-\Omega\right)\left[\frac{g\left(\mathbf{x}-\mathbf{x}'\right)}{\lambda f}+\frac{g\left(\mathbf{x}+\mathbf{x}'\right)}{\lambda f}\right]\Big\}.\end{aligned} \tag{68}$$

It can be noticed incidentally that in the limit of infinite aperture, one recovers the infinite resolution result of equation (28).

One can look for the limit cases where an asymptotic expression of the spectrum can be obtained. Let us first consider the case where the detection region $s_{\rm det}$ is quite large compared to the diffraction spot $s_{\rm diff}\sim(\lambda f)^2/(\pi\xi_0^2)$ of the aperture on the detector. In this case, because $g(\mathbf{x})$ varies on a spatial scale which is on the order of $\sqrt{s_{\rm diff}}$ (which is much smaller than the integration region), one may approximate the pupil frame function appearing in equation (68) by a delta function:

$$g\left(\mathbf{x}-\mathbf{x}'\right)\longrightarrow\lambda f\delta\left(\mathbf{x}-\mathbf{x}'\right). \tag{69}$$

Therefore, in this limit one finds the same result as in the case of infinite optical resolution given by equation (31), indepedentely of the radius of the aperture. On the other hand, let us consider the limit where the detection region $s_{\rm det}$ is much narrower than the diffraction spot $s_{\rm diff}$. In this case, the integrand in equation (68) can be considered as being constant and hence taken out of the integral. One then finds:

$$V\left(\Omega\right)\simeq N+\frac{s_{\rm det}}{s_{\rm diff}}S^{\rm PW}\left(\Omega\right), \tag{70}$$

where $S^{\rm PW}(\Omega)$ is the plane-wave result obtained in the case of infinite resolution.

References

1. L.A. Lugiato, A. Gatti, E. Brambilla, J. Opt. B: Quant. Semicl. Opt. **4** S183 (2002)
2. M.I. Kolobov, C. Fabre, Phys. Rev. Lett. **85**, 3789 (2000)
3. C. Fabre, J.B. Fouet, A. Maitre, Opt. Lett. **25**, 76 (2000)
4. N. Treps, U. Andersen, B. Buchler, P.K. Lam, A. Maitre, H. Bachor, C. Fabre, Phys. Rev. Lett. **88**, 203601 (2002)
5. I. Sokolov, M.I. Kolobov, A. Gatti, L.A. Lugiato, Opt. Commun. **193**, 175 (2001)
6. Special issue on Squeezed light, edited by R. Loudon, P.L. Knight, in J. Mod. Opt. **34**(6/7), (1987)
7. M.I. Kolobov, I.V. Sokolov, Sov. Phys. JETP **69**, 1097 (1989)
8. M.I. Kolobov, I.V. Sokolov, Europhys. Lett. **15**, 271 (1991)
9. A. La Porta, R.E. Slusher, Phys. Rev. A **44**, 2013 (1991); C. Kim, P. Kumar, Phys. Rev. Lett. **73**, 1605 (1994)
10. L.A. Lugiato, A. Gatti, Phys. Rev. Lett. **70**, 3868 (1993)

11. A. Gatti, L.A. Lugiato, Phys. Rev. A **52**, 1675 (1995)
12. A. Gatti, H. Wiedemann, L.A. Lugiato, I. Marzoli, G.L. Oppo, S.M. Barnett, Phys. Rev. A **56**, 877 (1997)
13. L.A. Lugiato, Ph. Grangier, J. Opt. Soc. Am. B **14**, 225 (1997)
14. S. Mancini, A. Gatti, L.A. Lugiato, Eur. Phys. J. D **12**, 499 (2000)
15. C. Schwob, P.F. Cohadon, C. Fabre, M.A.M. Marte, H. Ritsch, A. Gatti, L.A. Lugiato, Appl. Phys. B **66**, 685 (1998), special issue on Optical Parametric Oscillators, edited by J. Mlynek, S. Schiller
16. M. Marte, H. Ritsch, K.I. Petsas, A. Gatti, L.A. Lugiato, C. Fabre, D. Leduc, Opt. Expr. **3**, 71 (1998)
17. K.I. Petsas, A. Gatti, L.A. Lugiato, JEOS B: Quant. Semicl. Opt. **10**, 789 (1998)
18. A.E. Siegman, *Lasers* (University Science, Mill Valley, Calif., 1986)
19. L.A. Lugiato, G.-L. Oppo, J.R. Tredicce, L. Narducci, M.A. Pernigo, J. Opt. Soc. Am. B **7**, 1019 (1990); see also M. Abramowitz, I. Stegun, *Handbook of mathematical functions* (Dover NY, 1965), pp. 771–788
20. R. Bonifacio, L.A. Lugiato, Lett. Nuovo Cim. **21**, 505 (1978)
21. D.F. Walls, G.J. Milburn, *Quantum Optics* (Springer-Verlag, Berlin, 1994), pp. 127–128
22. C.W. Gardiner, M.J. Collett, Phys. Rev. A **31**, 3761 (1985)